ADVANCED HEALTHCARE MATERIALS
www.advhealthmat.de

Adhesive Wearable Sensors for Electroencephalography from Hairy Scalp

*Anan Zhang, Abhijith Balamuraleekrishna Shyam, Alexandra McCalla Cunningham, Christopher Williams, Amanda Brissenden, Alex Bartley, Brian Amsden, Aristides Docoslis, Marianna Kontopoulou, and Shideh Kabiri Ameri**

Electroencephalography has garnered interest for applications in mobile healthcare, human–machine interfaces, and Internet of Things. Conventional electroencephalography relies on wet and dry electrodes. Despite favorable interface impedance of wet electrodes and skin, the application of a large amount of gel at their interface with skin limits the electroencephalography spatial resolution, increases the risk of shorting between electrodes, and makes them unsuited for long-term mobile recording. In contrast, dry electrodes are better suited for long-term recordings but susceptible to motion artifacts. In addition, both wet and dry electrodes are non-adhesive to the hairy scalp and mechanical support, or chemical adhesives are used to hold them in place. Herein, a conical microstructure array (CMSA) based sensor made of carbon nanotube-polydimethylsiloxane composite is reported. The CMSA sensor is fabricated using the innovative, cost-effective, and scalable method of viscosity-controlled dip-pull process. The sensor adheres to the hairy scalp by generating negative pressure in its conical microstructures when it is pressed against scalp. Aided by the application of a trace amount of gel, CMSA sensor establishes good electrical contact with the skin, enabling its applications in mobile electroencephalography over extended periods. Notably, the signal quality of CMSA sensors is comparable to that of medical-grade wet gel electrodes.

1. Introduction

According to reports from the Global Burden of Disease (GBD) in 2019, neurological and mental disorders are the main causes of disability globally, and the top ten leading causes of burden worldwide.[1] Nearly one in six of the world's population lives with at least one type of such disease and disorder, and the numbers are expected to grow soon.[2,3] According to the World Health Organization (WHO), early detection of the brain and mental health disorders plays a major role in preventing and progression of these diseases.[4] Currently, diagnosis of brain and mental disorders demands expensive, bulky, and stationary equipment that contributes to the prevalence of late diagnoses. The most commonly used diagnostic tools for brain and mental disease and disorders are magnetoencephalography (MEG),[5] functional magnetic resonance imaging (fMRI),[6] electroencephalography (EEG),[7] and positron emission tomography (PET).[8] Among these technologies, EEG offers non-invasive measurement of the brain's electrical activities through placing electrodes on the scalp and is one of the primary diagnostic methods suited for portable and personal health care applications.[9] EEG is widely used in the diagnosis of epilepsy,[8] stroke,[10] dementia,[11] sleep, cognitive and mental disorders, etc., as it offers a high temporal resolution of milliseconds.[12–14] A visually imperceptible, miniaturized, and reliable EEG sensor-system that can be applied for long-term EEG recording during daily activities conveniently has

A. Zhang, A. B. Shyam, A. Bartley, S. K. Ameri
Department of Electrical and Computer Engineering
Queen's University
Kingston, Ontario K7L 3N6, Canada
E-mail: shideh.ameri@queensu.ca

The ORCID identification number(s) for the author(s) of this article can be found under https://doi.org/10.1002/adhm.202300142

DOI: 10.1002/adhm.202300142

A. M. Cunningham, C. Williams, A. Brissenden, B. Amsden, A. Docoslis, M. Kontopoulou
Department of Chemical Engineering
Queen's University
Kingston, Ontario K7L 3N6, Canada

S. K. Ameri
Centre for Neuroscience Studies (CNS)
Queen's University
Kingston, Ontario K7L 3N6, Canada

not been reported yet. Such technology offers a solution for the early diagnosis of neurological, brain, and mental disorders, and shows potential for applications in human–machine interfaces (HMI), artificial intelligence (AI), internet of things (IoT), and assistive technologies.[15–17]

Mobile EEG recording is challenging due to the difficulty of forming a stable interface between sensors and the microscopically rough surface of the scalp's skin, which is heavily covered with many hairs. This impacts the sensors' adhesion to the scalp, the interface impedance between the sensor and skin known as electrode–skin interface impedance (ESII), and the signal-to-noise ratio (SNR) of the recorded EEG signals.[18] Medical-grade EEG recording is usually performed using an array of silver/silver chloride (Ag/AgCl) electrodes held in place using an EEG cap. In order to obtain low ESII and high SNR, a relatively large amount of wet conductive gel (≈0.5 mL) is injected between the scalp and each electrode to ensure a good electrical connection at the skin–sensor interface.[19] This placement is time-consuming (usually 2–3 h), and it must be done in medical centres and hospitals by trained medical experts. Moreover, the spatial resolution of this recording method is low, and there is a high chance of shorting between closely spaced electrodes. For these reasons, this type of system is not suitable for mobile healthcare.[20]

An alternative recording option is using dry electrodes. Dry electrodes are made of conductive materials that are placed on the scalp and kept in place by mechanical support or the use of aggressive chemical adhesives.[20–24] The ESII of dry electrodes is comparatively higher than that of wet gel electrodes due to being non-conformal to the skin's texture, rendering them more prone to motion and significant motion artifacts[20] and limiting their application in mobile health care.

With the advances made in the synthesis of polymers with similar Young's modulus to that of skin, soft polymers coated with conductive films such as metals, nanowires, and graphene are used to fabricate soft, thin, and stretchable dry electrodes that can conform to the skin microscopic texture resulting in reduced motion artifacts and ESII.[16,25–29] However, recording EEG from hairy skin using thin planar electrodes is not possible since electrodes do not contact with the skin through dense hairs.[30,31]

Recently the application of conductive polymer composites in the fabrication of electrodes, and sensors for bio-signal recording has attracted attention due to the low cost, simplicity, and scalability of the fabrication process. The most widely used conductive fillers are metallic or carbon particles, carbon nanotubes (CNT), and nanowires.[32–38] To access the scalp beneath the hairs, dry electrodes consisting of large pillars on their surface are made of nano and metal particle-based polymer composites. However, without self-adhesion to the surface of the skin, mechanical support is required in order to maintain contact between electrodes, and scalp skin. This makes the electrodes uncomfortable, visually noticeable on the head, susceptible to motion and EEG recordings are greatly affected by motion-induced artifacts.[39–42] On the other hand, bio-inspired sensors with micropillars and gecko-inspired hierarchical structures made of nanomaterials-based polymer composites can adhere to hairless skin through Van Der Waal's force, but they are not capable of adhering to the hairy scalp.[43–47] This is because the diameter of the human hairs on the scalp is between 40 and 120 μm[48]—much larger than the size of aforementioned high-density micropillars or gecko-inspired structures that are usually only a few micrometers in diameter. Therefore, at the comparable scale to hairs' scale, these bio-inspired sensors are just similar to the sensors with planar geometries and the existence of hairs on the scalp impedes contact between such sensors, and the surface of the scalp. Recently, octopus-inspired or beetlelike self-adhesive sensors based on micro-suction-cup structures made of nanomaterials-based polymer composite have been developed, which again are not applicable to the hairy scalp.[49–51] Despite the wide application of polymer composites in bio-signal recording, to the best of our knowledge, there is currently no reliable dry electrode for mobile brain healthcare or wearables applications with the capability to adhere to hairy scalp or otherwise maintain conformal contact without the help of adhesives and/or mechanical support.[18,19]

Here, we report a novel CNT-PDMS composite-based sensor for EEG recording from the hairy scalp. This sensor consists of an array of stemmed conical microstructure arrays (CMSA) on its surface. The conical microstructures made on the surface of the sensor allow the sensor to attach to the skin regardless of the level of hair coverage. The CMSA sensors are fabricated using our innovative and unique, cost- and time-effective, scalable fabrication process we named the viscosity-controlled dip-pull process (VCDP). To fabricate the array of conical microstructures, the optimal viscosity of the polymer precursor was calibrated for optimal fine adjustment of the capillary rise of the polymer precursor within the mold during the fabrication of the CMSA sensors.

The CMSA sensor forms stable contact with the hairy scalp and makes good electrical contact with the skin by the application of a trace amount of conductive gel making the CMSA sensor suitable for long-term continuous EEG recording. The CMSA sensor was successfully used to measure electroencephalograms (EEG) from the hairy scalp as well as electrocardiograms (ECG) with comparable signal quality to the gold-standard medical grade wet gel electrodes.

2. Experimental Section

The CMSA sensor was fabricated using the innovative and unique, scalable, cost-effective VCDP process, illustrated in **Figure 1**. In this method, stemmed conical microstructure arrays were made by dipping a mold, consisting of an array of glass beads fixed on a glass slide, into a small pool of multiwall carbon nanotube (CNT)-polydimethylsiloxane (PDMS)-silicone oil (SO) precursor with adjusted viscosity. Once the glass beads were dipped to one-third of their radius in the precursor to form the conical heads of CMSA, the mold was pulled out gently to allow the elongation of the viscous precursor and the stems of the conical microstructures were formed. The viscosity of the precursor played a critical role in forming stems that facilitate the adhesion of the CMSA sensor to the hairy scalp. If the precursor has very low viscosity, the fast rise of polymer within the spaces between the glass beads in the mold due to capillary rise will result in failure to achieve proper stemmed structures; if the viscosity is very high, the elongation of precursor and formation of stems will not occur.

The CMSA sensor was made of a conductive polymer composite consisting of multiwall CNT as conductive fillers and PDMS as the polymer matrix. The fabrication process started with dispersing CNT in isopropanol alcohol (IPA). CNTs tended to

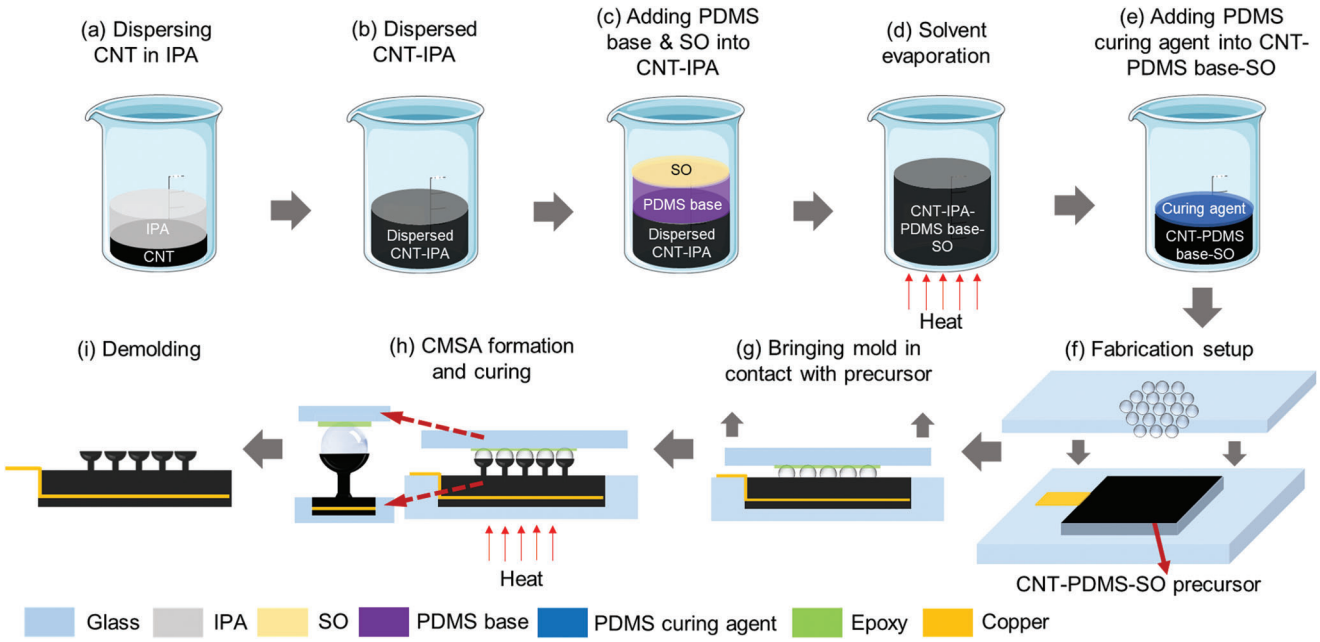

Figure 1. The fabrication process of the CMSA sensor. a) Dispersion of CNT in IPA via ultrasonication for 60 min. b) CNT temporarily suspended in IPA after ultrasonication. c) Silicone oil (SO) was added to CNT/IPA solution and ultrasonicated for 30 min, followed by the addition of PDMS base. d) IPA solvent is evaporated. e) The PDMS curing agent is added. f) CNT-PDMS-SO precursor poured into a reservoir. A copper stripe served as an electrical connection to the CMSA sensor. g) A mold consisting of an array of glass beads is dipped into the CNT-PDMS-SO precursor to form conical heads. h) The mold is raised up gently to form pillars. Then the precursor is heated to cure. i) The CMSA sensor is demolded once the CNT-PDMS-SO composite is fully cured.

aggregate in polymers and most chemical solvents due to van der Waals forces. In order to obtain a polymer composite with high electrical conductivity, CNTs should be dispersed well in the polymer matrix. IPA has been shown to improve the dispersion of CNTs within PDMS.[52] Based on the experiments, the CNT-IPA dispersion did not show any visible sign of sedimentation 3 days after dispersion.

In the first fabrication step, each milligram of CNT was dispersed in 0.5 mL of IPA using an ultrasonic bath for 60 min to form a well-dispersed CNT-IPA mixture (Figure 1a,b).[52] Next, low-viscosity (100 cSt), methyl group terminated (MEP) silicone oil (SO) was added to a CNT/IPA dispersion and ultrasonicated for 30 min, followed by addition of PDMS base and an additional 30 min of ultrasonication (Figure 1c). Methyl-terminated silicone oil coated the CNT surfaces, which has been shown to bring a more homogeneous dispersion of CNT in PDMS after IPA was evaporated. The silicone oil interacted with the hydrophobic surface of the CNTs to create a thermodynamically stable CNT dispersion in PDMS.[53]

The concentration of silicone oil and the weight percentage (wt.%) of CNT were adjusted carefully to obtain good electrical conductivity as well as optimum viscosity that suits the developed VCDP fabrication process. In order to obtain optimal viscosity of polymer precursor for the fabrication of the CMSA sensor, the capillary rise of PDMS precursors was studied with different viscosities. The analysis results suggested that viscosity of over 2000 Pa s was required in order to fabricate proper microstructures using the VCDP fabrication process (Figure S1, Supporting Information). A CNT-PDMS-SO precursor with proper viscosity and conductivity was obtained by mixing 2.4 wt.% of CNT (Cheap Tubes, Multi-Wall Carbon Nanotubes 10–20 nm) and silicone oil (Sigma–Aldrich, 63 148) in PDMS (Sylgard 184), with CNT to SO weight ratio of 1:8. Figure S2 (Supporting Information) shows that the viscosity of the CNT-PDMS-SO precursor increases by increasing the weight ratio of CNT, with the CNT to SO weight ratio fixed to be 1:8. This CNT-PDMS-SO precursor with 2.4 wt.% CNT was tested with the viscosity of ≈12 654 Pa s after adding curing agent. **Figure 2**a shows the electrical conductivity increased by increasing the CNT contents. The sheet resistance was measured to be 1.387 KΩ sq^{-1} at 2.4 wt.% of CNT with the CNT to SO weight ratio of 1:8 (Figure 2a).

After preparation of CNT-PDMS-base-SO, the mixture was heated at 50 °C to evaporate IPA solvent (Figure 1d). The temperature was kept below the boiling point of IPA to prevent the formation of microbubbles that could degrade the electrical and mechanical properties of the composite. In the next step, the PDMS curing agent with a 1:10 weight ratio of the PDMS base was added to the mixture (Figure 1e). Then, the CNT-PDMS-SOprecursor was placed in a vacuum chamber for de-bubbling.

The fabrication setup consisted of two parallel stages. The first was the fixed stage with a reservoir for polymer composite precursor and was equipped with a controllable heating system and a microscope camera to monitor the process. The other stage was the movable stage that had movability in x–y–z directions (with 2 µm resolution in the z-direction) that acted as a mold holder (Figure 1f). To form conical microstructure arrays, a mold was made using an array of 1.5 mm diameter borosilicate glass beads secured on a glass slide by epoxy glue. A layer of releasing agent was sprayed over the mold to ease the demolding of the microstructures. The mold, which was initially spaced from the

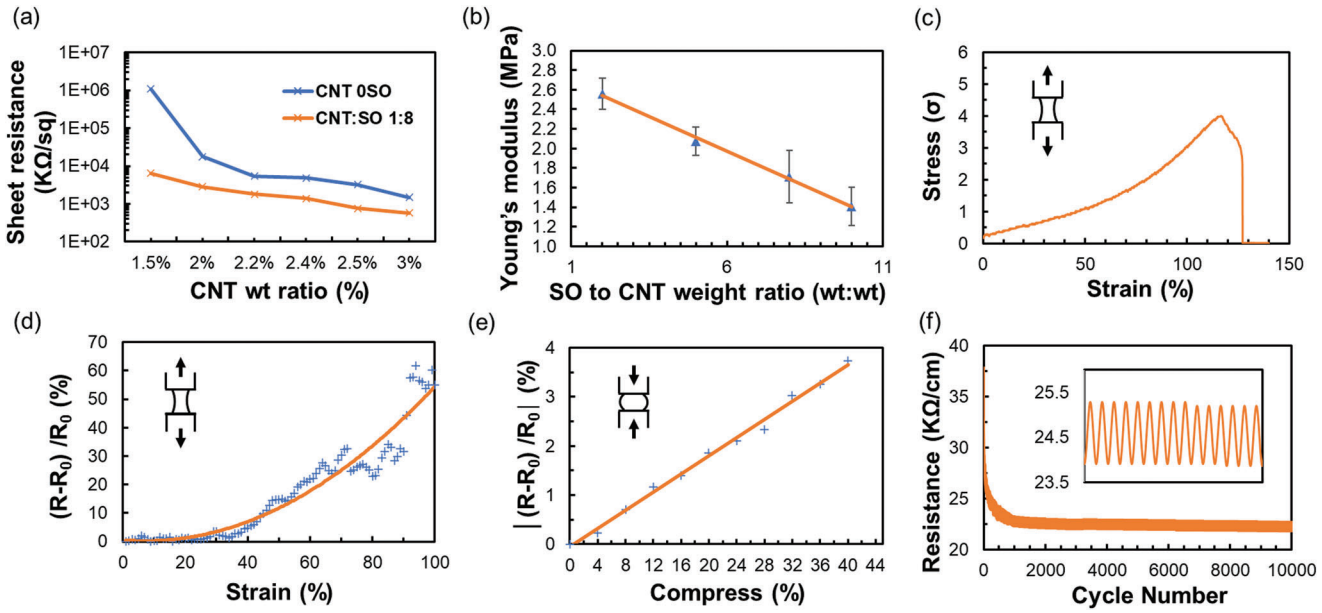

Figure 2. Electrical and mechanical characteristics of CNT-PDMS-SO polymer. a) Sheet resistance of CNT-PDMS-SO polymer samples consisting of different CNT weight percentages with and without SO. The weight ratio of CNT to SO in the composition of polymer composite containing SO was 1:8. b) Young's modulus of CNT-PDMS-SO polymer samples consisting of different CNT to SO weight ratios. c) Normalized stress–strain curve of CNT-PDMS-SO polymer consisting of 2.4 wt.% CNT with CNT to SO weight ratio of 1:8 versus applied tensile strain. d) Normalized resistance changing curve of CNT-PDMS-SO polymer consisting of 2.4 wt.% CNT with CNT to SO weight ratio of 1:8 versus applied tensile strain. e) Normalized resistance changing curve of CNT-PDMS-SO polymer consisting of 2.4 wt.% CNT with CNT to SO weight ratio of 1:8 versus applied compression. In (d) and (e), the blue crosses are the experimental data, and the orange lines are the fitted curves. f) CNT-PDMS-SO polymer consisting of 2.4 wt.% CNT with CNT to SO weight ratio of 1:8 under cyclic tensile strain of 20% for 10 000 cycles.

precursor reservoir, was lowered in the *z*-direction and dipped into the CNT-PDMS-SO precursor to form conical heads (Figure 1g). Once glass beads were dipped to a depth of one-third of their radius in the precursor, the mold was raised up gently to form pillars with the desired height and width (Figure 1h). In the next step, the precursor was heated at 100 °C to fully cure the polymer composite precursor (Figure 1h). Finally, when the CNT-PDMS-SO composite was fully cured, the CMSA sensor was demolded (Figure 1i). The human subject study was performed under Queen's University Health Sciences & Affiliated Teaching Hospitals Research Ethics Board (HSREB) approval (number 6027092).

3. Results and Discussion

The CNT-PDMS-SO polymer composite's electrical and mechanical characteristics were studied for CNT weight percentages between 1.5% and 3%, with a CNT-to-SO weight ratio of 1:8. Figure 2a shows that the sheet resistance of the polymer composite decreases significantly by increasing the weight percentage of CNT significantly after achieving the percolation with 1.5–2 wt.% of CNT.

The Young's modulus of the CNT-PDMS-SO composite increases with the increasing weight percentage of CNT, and functionalization with low viscosity silicone oil reduces the elastic modulus of polymer composite (Figure 2b; Figure S3, Supporting Information). Increasing the weight percentage of CNT reduces the electrical resistivity but increases Young's modulus. The optimal combination of sufficient electrical conductivity and proper mechanical softness of the polymer composite was obtained at 2.4 wt.% of CNT with the CNT to SO weight ratio of 1:8. The mechanical characterization of this CNT-PDMS-SO polymer sample indicates a Young's modulus of 1.717 MPa (Figure 2c) and a fracture strain of 116%.

Figure 2d shows the change in the electrical resistance of polymer composites consisting of 2.4 wt.% of CNT and a CNT-to-SO weight ratio of 1:8 (used to eventually fabricate CMSA sensor), due to applied uniaxial tensile strain. Less than 5% of resistance change was detected within 40% of applied strain that is well beyond the stretchability of human skin (≈30%). Additionally, a compression test on the CNT-PDMS-SO polymer (2.4% CNT, CNT to SO 1:8) was performed, indicating < 4% of resistance change due to 40% of applied compression (Figure 2e). The normalized change in electrical resistance of this polymer composite under the applied cyclic tensile strain of 20% is demonstrated for 10000 cycles in Figure 2f. Over the first 100 cycles, an irreversible decrease of composite's electrical resistance is observed, which eventually stabilized after ≈1000 cycles of tensile strain. This can be attributed to changes in the interconnected network of CNTs in the polymer matrix. After enough strain cycles, the breaking and reforming of the CNT networks in the polymer matrix become more consistent and the resistance stabilizes.[53] Therefore, 100 cycles of strain and compression were applied to the CMSA sensor before the recording.

Figure 3a shows the schematic of both CMSA sensors and planar conventional wet gel electrodes. Conventional wet gel electrodes require a relatively a large amount of gel (≈0.5 mL) between the electrode and skin to establish electrical contact,

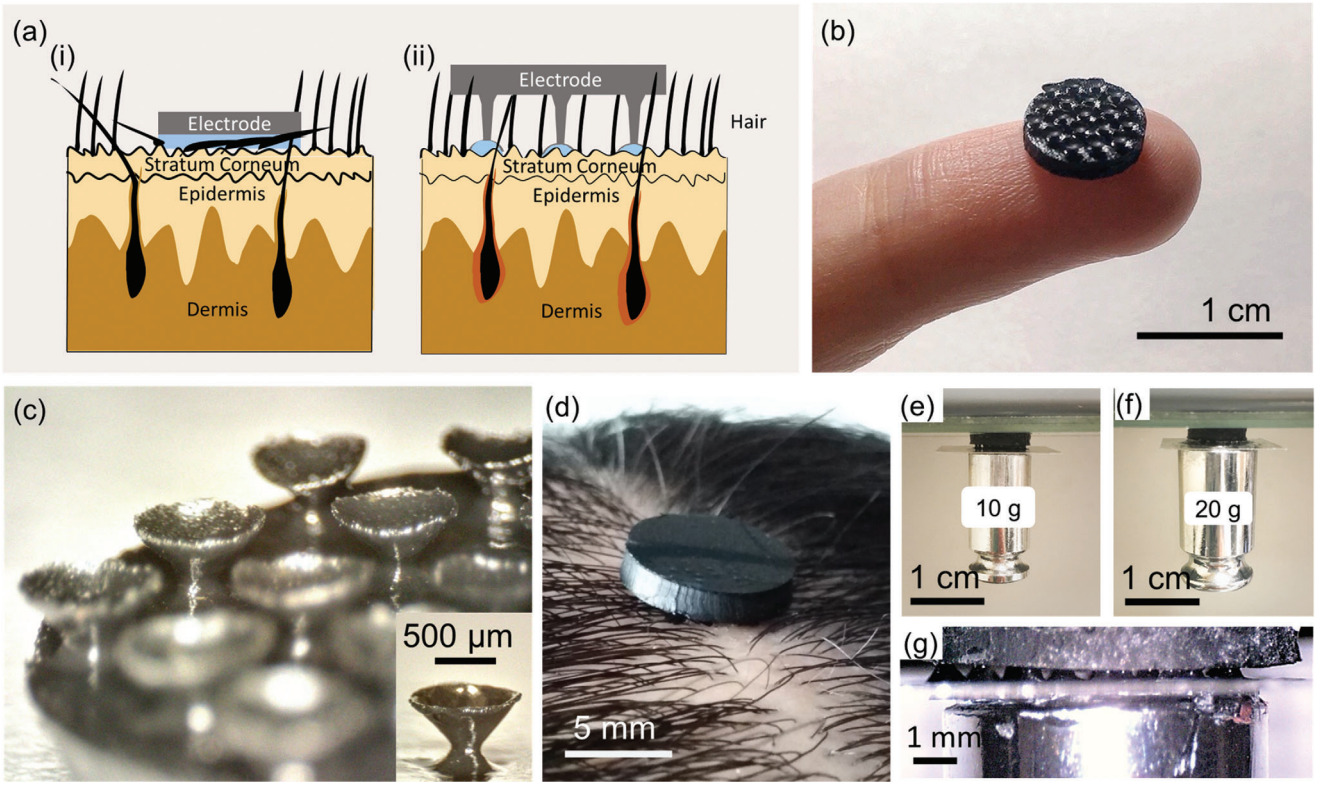

Figure 3. Fabricated the CMSA sensor. a) A schematic of medical grade electrodes for EEG recording with wet gel applied between electrodes with planar geometry and microscopically textured hairy scalp and the CMSA sensor on the hairy scalp (blue represents wet gel). b) The CMSA sensor was placed on the fingertip. c) Microscopic image of the CMSA sensor. d) The CMSA sensor attached on hairy scalp. e) Demonstration of the CMSA sensor suction force to a glass slide without applying wet gel and f) suction force to a glass slide with applying gel on conical heads of microstructures. g) Microscopic image of the interface between the CMSA sensor and glass surface without applying the wet gel.

resulting in limited spatial resolution, the necessity of using mechanical support to keep the electrodes in place, and a high chance of electrodes shorting when in the array due to running the gel. In contrast, the design of the CMSA sensor enables direct contact and the adhesion of the sensor to the hairy skin. The small size of the sensor (8 mm in diameter) allows for non-intrusive applications for EEG recording from the scalp (Figure 3b).

Each microstructure in a CMSA sensor consists of an array of stemmed conical structures that make it possible to position the conical heads in the space between hair strands on the scalp and hairy skin. By gently pressing the CMSA sensor against the skin and pushing the air out of conical heads, a negative pressure is generated that causes the CMSA sensor to adhere to the skin. To ensure low ESII, a trace amount of conductive gel (≈5 µL) is applied to the inner surfaces of the conical heads before each application. As shown in Figure 3b, each CMSA sensor consists of a base with a radius of 8 mm and a thickness of 1.5 mm where the arrays of 19 conical microstructures are located. Unlike planar conventional wet gel electrodes, the CMSA sensors require little gel, making them easy to be attached to the scalp and comfortable to wear. Additionally, they can adhere to the hairy scalp without the help of mechanical support and can be visually imperceptible due to their small size and the fact that there is no need for extra accessories to hold them in place (Figure 3d).

The microstructure in the CMSA sensor is shown in Figure 3c. Each microstucture consists of a stem with a radius of 150 ± 20 µm and a height of 300 ± 20 µm and a conical head with a radius of 450 ± 20 µm.

The soft conical heads in the CMSA sensor enable the adhesion of the CMSA sensor to both smooth and textured surfaces such as glass and skin respectively (Figure S4a,b, Supporting Information). Video S1 (Supporting Information) demonstrates that by pressing a stemmed conical head against the skin, a negative pressure is generated in the conical microstructure that results in adhesion to the skin. Application of the CMSA sensor to the hairy scalp is easy, and as Video S2 (Supporting Information) shows, once it is placed on the scalp, it stays intact even during intense head movements. Video S3 (Supporting Information) demonstrates the visual imperceptibility of the CMSA sensor offering users privacy, especially during long-term EEG recording during daily activities. The maximum adhesion forces of a CMSA sensor consisting of an array of 19 conical microstructures to a glass surface with and without the application of wet gel were measured to be 201 mN (0.4 N cm^{-2}) and 103 mN (0.2 N cm^{-2}), respectively (Figure 3e,f). Figure 3g shows the image of the interface between conical microstructures and glass surfaces. When the skin surface is dry, the adhesion force of the CMSA sensor attached to non-hairy scalp/skin with and without gel is 180 mN (360 mN cm^{-2}) and 40 mN (80 mN cm^{-2}), respectively. The adhesion force of the CMSA sensor attached to the hairy scalp with and without gel is 130 mN (260 mN cm^{-2}) and 35 mN (70 mN cm^{-2}), respectively. There is a slight decrease

in the adhesion force of the CMSA sensor attached to the hairy scalp compared to the non-hair skin, which is mainly due to the topology of the scalp and the elasticity of the hair. When the skin surface is wet due to sweating, the adhesion force of the CMSA sensor attached to non-hairy skin with and without gel is 190 mN (380 mN cm^{-2}) and 45 mN (90 mN cm^{-2}), respectively, and the adhesion force of the CMSA sensor attached to the hairy scalp with and without gel is 135 mN (270 mN cm^{-2}) and 40 mN (80 mN cm^{-2}), respectively. We did not notice a considerable change in the adhesion between the CMSA sensor and the skin when the person is sweating. This can be attributed to the absorption of sweat by the gel.

Figure S5 (Supporting Information) demonstrates that the adhesion force of CMSA sensors increases with an increase in the radius of the conical heads. The adhesion strength of the CMSA sensor is proportional to the size of the conical heads and the negative pressure generated in the conical heads when the air is pressed out. Based on multiple tests of the suction forces of conical heads array with different conical head radius, we calculated the suction force of the CMSA sensor consisting of 19 conical heads (without gel; Figure S5c, Supporting Information). The difference between the measured and calculated values is attributed to the deviation of the conical microstructures from their ideal shape and form, the slight nonuniformity of the radius of the cups and the leakage of air into the cups due to the minimal conformability of the cups to the attaching surface. Also, when the conical microstructure is pressed against a surface, there is an area at the center of it that does not come into contact with the surface as shown in Figure S5a (Supporting Information). Adding conductive gel (highlighted in blue in Figure S5b, Supporting Information) results in increasing the contact area between the skin and the sensor and consequently decreasing the electrode–skin interface impedance (ESII). There is a trade-off between the sensor's adhesion force and the radius of conical heads in CMSA sensors because these structures must be small enough to fit within the spacing between hair follicles (500 μm to 1 mm in most of the human scalp; Figure S6, Supporting Information).

The defining factor in obtaining high SNR and high-quality bio-signal recording is low ESII. We measured the CMSA sensor's ESII and compared it with gold standard medical grade Ag/AgCl wet gel electrodes. Impedance measurements were performed by placing the electrodes on the forearm and connecting them to an LCR meter (**Figure 4**a). The sweep frequency was set between 20 Hz and 100 kHz. The results shown in Figure 4b suggest that the ESII of Ag/AgCl wet gel electrodes at their interface with skin is lower than that of CMSA sensors. However, one must note that classical electrical circuit concepts suggest that the ESII is inversely proportional to the contact surface area of sensor/electrodes with skin. Considering that the contact surface area of the CMSA sensor with skin is only ≈0.121 cm^2 in comparison with that in wet gel electrode that is ≈2.54 cm^{-2} (21 times that of the CMSA sensor), the ESII per unit surface area of the CMSA sensor is lower than the wet-gel electrode. The ESII reduces with increasing frequency, indicating the capacitive nature of the interface between the sensor/electrode with the skin.

To investigate the performance of the CMSA sensor for electrophysiological recording, it was used to record EEG and ECG signals. Sensor placement on the chest for ECG recording is shown in Figure 4c. Medical grade Ag/AgCl wet gel electrodes (3M electrodes) were placed next to the CMSA sensors and used to measure the ECG signal concurrently for comparison. A trace amount of wet gel was applied to the inner surface of the CMSA sensor's conical heads (≈5 μL) prior to attaching the sensors to the chest. An OpenBCI board was used for data acquisition, and a digital 60 Hz notch filter was applied to the recorded data. Figure 4d depicts the simultaneous recording of ECG signals using the CMSA sensors and gold standard Ag/AgCl wet electrodes, with closely comparable results. The ECG signals obtained using the CMSA sensor include feature the distinctive P, Q, R, S, and T ECG peaks. The SNR of signals recorded using CMSA sensors and wet gel Ag/AgCl electrodes was measured to be 13.74 and 14.03, respectively. The ECG signal recording continued 6 h after the placement of sensors, and the results suggest a comparable decline of 15.8% and 18.1% in the SNR of the signals recorded using Ag/AgCl electrodes and CMSA sensors, respectively, due to the drying out the wet gel over time.

One critical aspect of wearable technology sensors is their comfort and non-irritability, particularly during prolonged use. To investigate this, we placed the CMSA sensor and Ag/AgCl wet gel electrode on the forearm and looked for any signs of irritation 6 h after placement on the skin. We observed that the CMSA sensor did not cause any irritation after 6 h of wear, while wet gel electrodes caused redness and irritation (Figure S7, Supporting Information). Furthermore, their small size, lightweight and simple application make it a comfortable and user-friendly sensor.

To assess its susceptibility to motion artifacts, the CMSA sensor and Ag/AgCl wet gel electrodes were placed in close proximity on the chest (**Figure 5**a,b) and simultaneous ECG recordings were performed while the motion was induced by poking skin in the vicinity of both sensors using a glass rod. A 60 Hz notch filter and a high-pass filter of 1 Hz were applied to the recorded signal. The result indicates that CMSA sensors show comparable motion artifacts to gold standard medical grade wet gel Ag/AgCl electrodes (Figure 5c).

We also used the CMSA sensor for EEG recording from the scalp. The alpha rhythm (8–13 Hz) was measured using the CMSA sensor and Ag/AgCl wet gel electrodes simultaneously from both forehead (Figure 4e) and hairy scalp at F4 position (Figure 4i) based on the 10–20 EEG measurement system. Reference and ground electrodes were placed on the A1 position and wrist.[54,55] To record the alpha rhythm, the subject was asked to hold their eyes open for 30 s followed by another 30 s when they were asked to close their eyes and relax. The recorded EEG signals in the time domain are shown in Figure 4f,j. Our results show the CMSA sensor can be used to record EEG signals from both the forehead and hairy scalp. The corresponding fast Fourier transform (FFT) results of the recorded signals when the eyes were open and closed are presented in Figure 4g,h,k,l. Our results show clear alpha signals recorded using both the CMSA sensor and Ag/AgCl wet gel electrodes at a peak frequency of ≈10 Hz during the period when the eyes were closed.

To study the stability of the CMSA sensor contact with skin during physical activities, one CMSA sensor was worn on the scalp and another sensor on the chest by a subject. The subject then did workout by running on a treadmill at the speed of 6.5 mph for 25 min (Video S5, Supporting Information). The CMSA sensors' contact with the skin on the scalp and chest remained

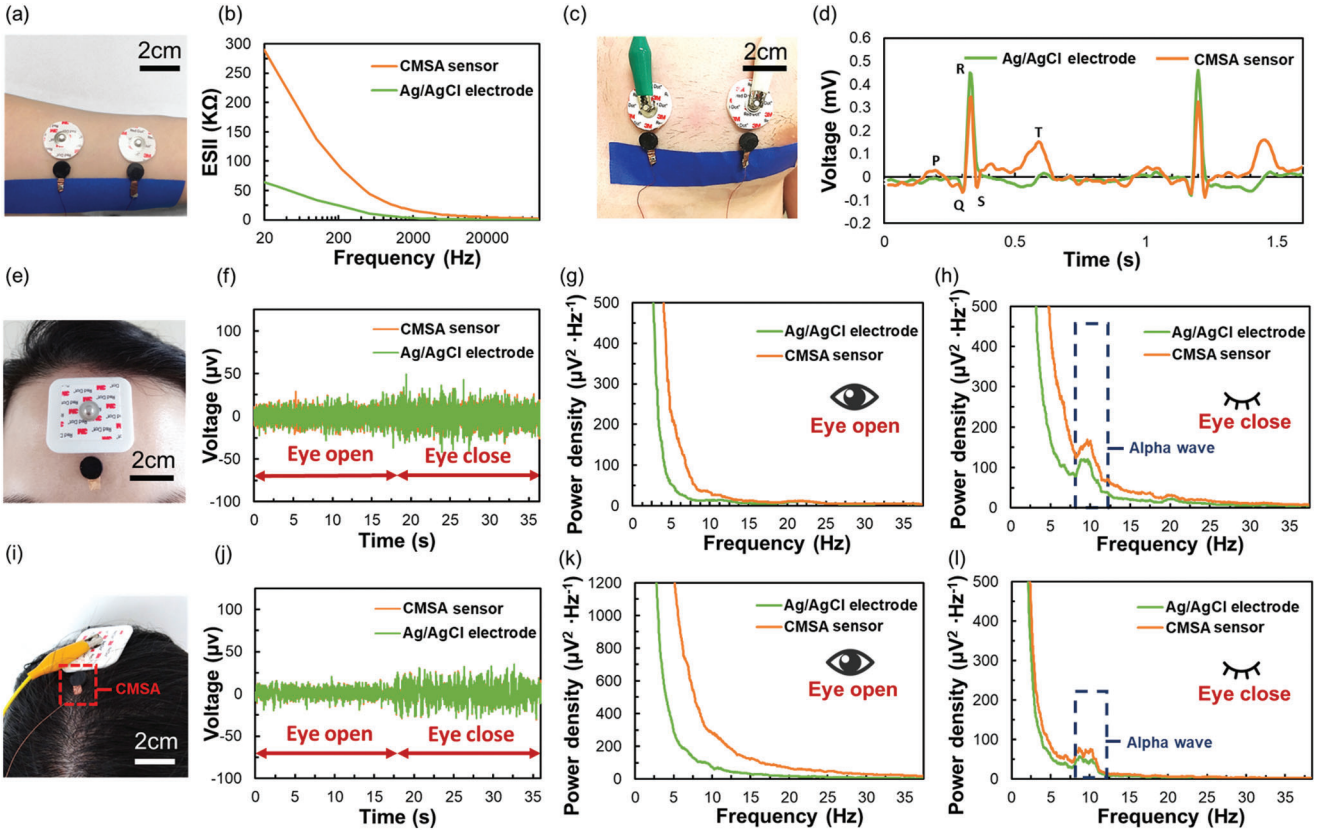

Figure 4. Electrical performance of the CMSA sensor on skin. a,b) Comparison of electrode-skin interface impedance of the CMSA sensor and commercial Ag/AgCl wet electrodes without any skin preparation. c) The placement of the CMSA sensors and gold standard Ag/AgCl electrodes on chest. d) ECG recording from the chest using both the CMSA sensors and Ag/AgCl wet gel electrodes. e) The placement of the CMSA sensors and gold standard Ag/AgCl electrodes on forehead. f) Recording the alpha rhythm from the forehead with both the CMSA sensor and Ag/AgCl wet gel electrodes. g,h) Comparison of EEG signals detected when eyes were open and closed, respectively. When the eyes were closed, an Alpha rhythm of 8–12 Hz was detected by both electrodes. i) The placement of the CMSA sensors and gold standard Ag/AgCl electrodes on hairy scalp (F4 position). j) alpha rhythm detection from the hairy scalp with both the CMSA sensor and gel electrodes. k,l) Comparison of EEG signal detected when eyes were open and closed respectively. When the eyes were closed, an Alpha rhythm of 8–12 Hz was detected by both electrodes.

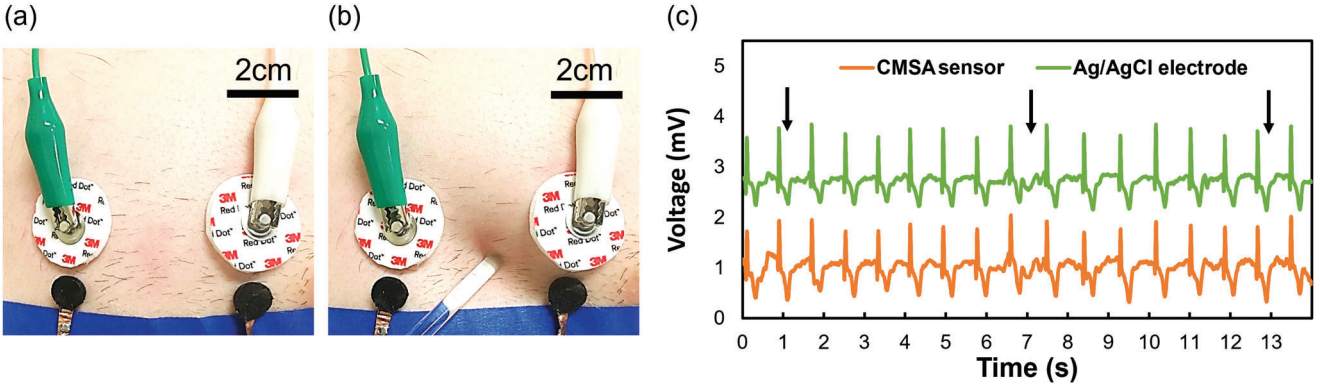

Figure 5. The comparison of motion artifacts of the CMSA sensor and Ag/AgCl wet electrodes. a) The placement of the CMSA sensors and gold standard Ag/AgCl electrodes on the chest. b) The motion was induced by poking the chest using a glass rod. c) ECG synchronously recorded by the CMSA sensors and Ag/AgCl wet electrodes shows comparable susceptibility to motion.

intact. We conducted the ECG recording using the CMSA sensors before and after the workout and we did not observe any noticeable change in the average ECG signal amplitude (Figure S8, Supporting Information). The long-term adherability of the CMSA sensor on the hairy scalp was tested by attaching it to the hairy scalp without the help of external mechanical support or tape while the EEG signal was measured continuously for 6 h. The first obvious degradation in the signal quality was observed after 4h due to the separation of some of the conical heads from the skin. Signal quality was restored by gently pressing the sensor against the skin to re-establish the contact between separated conical heads and skin. The recording then continued for another 2 h. The CMSA sensor can be reused by rinsing it with water and re-applying the conductive gel before the next use. There are no noticeable changes in the integrity of the CMSA sensor after rinsing it with water and reusing it after 30 cycles, as it is shown in Figure S10 (Supporting Information).

4. Conclusions

We developed a CNT-PDMS-SO based conical microstructure array (CMSA) sensor using an innovative and unique, scalable, cost- and time-effective fabrication method of viscosity-controlled-dip-pull (VCDP). The CMSA sensor can be attached directly to the skin that is heavily covered by hair such as the scalp without the help of any mechanical support and/or tape and has been successfully used for ECG recording and EEG recording from the hairy scalp. The quality of signals recorded by the CMSA sensor is comparable to medical grade, gold standard Ag/AgCl wet gel electrodes. The CMSA sensor is a wearable sensor that offers comfort and privacy to users for long-term EEG recording. The small size and adhesiveness of the CMSA sensor make it an excellent candidate for integration with integrated circuits at each sensor node on the scalp and potentially a candidate for the next generation of wireless visually imperceptible EEG sensors.

Supporting Information

Supporting Information is available from the Wiley Online Library or from the author.

Acknowledgements

This work was supported by the Natural Sciences and Engineering Research Council of Canada (NSERC), under the PI's and AD's NSERC Discovery Grant and the Queen's University Dean's Research Fund. After initial online publication, the caption to Figure 3b was corrected on June 21, 2023, due to a previous typing error.

Conflict of Interest

The authors declare no conflict of interest.

Data Availability Statement

Research data are not shared.

Keywords

CNT PDMS nanocomposites, dry electroencephalography (EEG) electrodes, self adhesive electrodes, wearables

Received: January 12, 2023
Revised: March 23, 2023
Published online: June 9, 2023

[1] GBD 2019 Mental Disorders Collaborators, *Lancet Psychiatry* **2022**, *9*, 137.
[2] World Health Organization, *Mental Health and COVID-19: Early Evidence of the Pandemic's Impact: Scientific Brief*, WHO, Geneva, Switzerland **2022**.
[3] A. Avan, H. Digaleh, M. Di Napoli, S. Stranges, R. Behrouz, G. Shojaeianbabaei, A. Amiri, R. Tabrizi, N. Mokhber, J. D. Spence, *BMC Med.* **2019**, *17*, 1.
[4] E. J. Costello, *J. Clin. Child. Adolesc. Psychol.* **2016**, *45*, 710.
[5] S. Baillet, *Nat. Neurosci.* **2017**, *20*, 327.
[6] J. Hennig, O. Speck, M. A. Koch, C. Weiller, *J. Magn. Reson. Imaging* **2003**, *18*, 1.
[7] A. Biasiucci, B. Franceschiello, M. M. Murray, *Curr. Biol.* **2019**, *29*, R80.
[8] J. Pillai, M. R. Sperling, *Epilepsia* **2006**, *47*, 14.
[9] T. L. Schultz, *Neurodiagn. J.* **2012**, *52*, 69.
[10] J. Wu, R. Srinivasan, E. Burke Quinlan, A. Solodkin, S. L. Small, S. C. Cramer, *J. Neurophysiol* **2016**, *115*, 2399.
[11] D. Adamis, S. Sahu, A. Treloar, *Int. J. Geriatr. Psychiatry* **2005**, *20*, 1038.
[12] M. M. Siddiqui, G. Srivastava, S. H. Saeed, *Sleep. Sci.* **2016**, *9*, 186.
[13] S. Debener, M. Ullsperger, M. Siegel, A. K. Engel, *Trends Cogn. Sci.* **2006**, *10*, 558.
[14] M. Soufineyestani, D. Dowling, A. Khan, *Appl. Sci.* **2020**, *10*, 7453.
[15] S. K. Ameri, M. Kim, I. A. Kuang, W. K. Perera, M. Alshiekh, H. Jeong, U. Topcu, D. Akinwande, N. Lu, *npj 2D Mater. Appl.* **2018**, *2*, 19.
[16] L. M. Ferrari, U. Ismailov, J.-M. Badier, F. Greco, E. Ismailova, *npj Flexible Electron.* **2020**, *4*, 4.
[17] J. J. Norton, D. S. Lee, J. W. Lee, W. Lee, O. Kwon, P. Won, S.-Y. Jung, H. Cheng, J.-W. Jeong, A. Akce, *Proc. Natl. Acad. Sci. USA* **2015**, *112*, 3920.
[18] E. H. T. Shad, M. Molinas, T. Ytterdal, *IEEE Sens. J.* **2020**, *20*, 14565.
[19] G. Li, S. Wang, Y. Y. Duan, *Sens. Actuators, B* **2018**, *277*, 250.
[20] G. Li, S. Wang, Y. Y. Duan, *Sens. Actuators, B* **2017**, *241*, 1244.
[21] L. Zhang, K. S. Kumar, H. He, C. J. Cai, X. He, H. Gao, S. Yue, C. Li, R. C.-S. Seet, H. Ren, *Nat. Commun.* **2020**, *11*, 1.
[22] S. M. Lee, J. H. Kim, H. J. Byeon, Y. Y. Choi, K. S. Park, S.-H. Lee, *J. Neural. Eng.* **2013**, *10*, 036006.
[23] J. S. Lee, C. M. Han, J. H. Kim, K. S. Park, *Electron. Lett.* **2015**, *51*, 1643.
[24] S. M. Lee, J. H. Kim, C. Park, J.-Y. Hwang, J. S. Hong, K. H. Lee, S. H. Lee, *IEEE Trans. Biomed. Eng.* **2015**, *63*, 138.
[25] S. Kabiri Ameri, R. Ho, H. Jang, L. Tao, Y. Wang, L. Wang, D. M. Schnyer, D. Akinwande, N. Lu, *ACS Nano* **2017**, *11*, 7634.
[26] P. Leleux, J. M. Badier, J. Rivnay, C. Benar, T. Herve, P. Chauvel, G. G. Malliaras, *Adv. Healthcare Mater.* **2014**, *3*, 490.
[27] D.-H. Kim, N. Lu, R. Ma, Y.-S. Kim, R.-H. Kim, S. Wang, J. Wu, S. M. Won, H. Tao, A. Islam, *Science* **2011**, *333*, 838.
[28] L. Wang, S. Qiao, S. Kabiri Ameri, H. Jeong, N. Lu, *J. Appl. Mech.* **2017**, *84*, 111003.
[29] Y. Wang, Y. Qiu, S. K. Ameri, H. Jang, Z. Dai, Y. Huang, N. Lu, *npj Flexible Electron.* **2018**, *2*, 6.
[30] C. Xu, Y. Yang, W. Gao, *Matter* **2020**, *2*, 1414.

[31] D. Kireev, S. K. Ameri, A. Nederveld, J. Kampfe, H. Jang, N. Lu, D. Akinwande, *Nat. Protoc.* **2021**, *16*, 2395.
[32] B. Liu, H. Tang, Z. Luo, W. Zhang, Q. Tu, X. Jin, *Sens. Actuators, A* **2017**, *265*, 79.
[33] J. Jung, S. Shin, Y. T. Kim, *Microelectron. Eng.* **2019**, *203*, 25.
[34] B. Sun, R. N. McCay, S. Goswami, Y. Xu, C. Zhang, Y. Ling, J. Lin, Z. Yan, *Adv. Mater.* **2018**, *30*, 1804327.
[35] L. Liu, H. Y. Li, Y. J. Fan, Y. H. Chen, S. Y. Kuang, Z. B. Li, Z. L. Wang, G. Zhu, *Small* **2019**, *15*, 1900755.
[36] Z. Jiang, M. O. G. Nayeem, K. Fukuda, S. Ding, H. Jin, T. Yokota, D. Inoue, D. Hashizume, T. Someya, *Adv. Mater.* **2019**, *31*, 1903446.
[37] W. Guo, P. Zheng, X. Huang, H. Zhuo, Y. Wu, Z. Yin, Z. Li, H. Wu, *ACS Appl. Mater. Interfaces* **2019**, *11*, 8567.
[38] S. M. Lee, H. J. Byeon, J. H. Lee, D. H. Baek, K. H. Lee, J. S. Hong, S.-H. Lee, *Sci. Rep.* **2014**, *4*, 1.
[39] Y.-H. Chen, M. O. d. Beeck, L. Vanderheyden, V. Mihajlović, B. Grundlehner, C. V. Hoof, in *35th Annual International Conference of the IEEE Engineering in Medicine and Biology Society (EMBC)*, IEEE, New York, USA **2013**, 551
[40] K.-P. Gao, H.-J. Yang, X.-L. Wang, B. Yang, J.-Q. Liu, *Sens. Actuators, A* **2018**, *283*, 348.
[41] P. Li, J. Huang, M. Li, H. Li, *Sens. Actuators, A* **2022**, *340*, 113547.
[42] M. Kimura, S. Nakatani, S. I. Nishida, D. Taketoshi, N. Araki, *Sensors* **2020**, *20*, 4733.
[43] C. Greiner, A. D. Campo, E. Arzt, *Langmuir* **2007**, *23*, 3495.
[44] F. Stauffer, M. Thielen, C. Sauter, S. Chardonnens, S. Bachmann, K. Tybrandt, C. Peters, C. Hierold, J. Vörös, *Adv. Healthcare Mater.* **2018**, *7*, 1700994.
[45] W. G. Bae, D. Kim, M. K. Kwak, L. Ha, S. M. Kang, K. Y. Suh, *Adv. Healthcare Mater.* **2013**, *2*, 109.
[46] M. Seong, I. Hwang, J. Lee, H. E. Jeong, *Sensors* **2020**, *20*, 6975
[47] T. Kim, J. Park, J. Sohn, D. Cho, S. Jeon, *ACS Nano.* **2016**, *10*, 4770.
[48] H. Kang, T. W. Kang, S. D. Lee, Y. M. Park, H. O. Kim, S. Y. Kim, *Int. J. Dermatol.* **2009**, *48*, 14.
[49] S. Chun, W. Son, D. W. Kim, J. Lee, H. sMin, H. Jung, D. Kwon, A.-H. Kim, Y.-J. Kim, S. K. Lim, *ACS Appl. Mater. Interfaces* **2019**, *11*, 16951.
[50] H. Min, S. Jang, D. W. Kim, J. Kim, S. Baik, S. Chun, C. Pang, *ACS Appl. Mater. Interfaces* **2020**, *12*, 14425.
[51] S. Baik, J. Lee, E. J. Jeon, B.-y. Park, D. W. Kim, J. H. Song, H. J. Lee, S. Y. Han, S.-W. Cho, C. Pang, *Sci. Adv.* **2021**, *7*, eabf5695.
[52] C.-X. Liu, J.-W. Choi, *Nanomaterials* **2012**, *2*, 329.
[53] J. H. Kim, J.-Y. Hwang, H. R. Hwang, H. S. Kim, J. H. Lee, J.-W. Seo, U. S. Shin, S.-H. Lee, *Sci. Rep.* **2018**, *8*, 1.
[54] T. Kawada, Y. Kiryu, S. Aoki, S. Suzuki, *Psychiatry Clin. Neurosci.* **1992**, *46*, 937.
[55] E. Olejarczyk, P. Bogucki, A. Sobieszek, *Front Neurosci.* **2017**, *11*, 506.